Acta Oceanol. Sin., 2020, Vol. 39, No. 11, P. 52–68
https://doi.org/10.1007/s13131-020-1670-5
http://www.hyxb.org.cn
E-mail: hyxbe@263.net

Kuroshio intrusion in the Luzon Strait in an eddy-resolving ocean model and air-sea coupled model

Qian Yang[1, 2], Hailong Liu[1, 2*], Pengfei Lin[1, 2], Yiwen Li[1, 2]

[1] State Key Laboratory of Numerical Modeling for Atmospheric Sciences and Geophysical Fluid Dynamics, Institute of Atmospheric Physics, Chinese Academy of Sciences, Beijing 100029, China

[2] College of Earth Sciences, University of Chinese Academy of Sciences, Beijing 100049, China

Received 13 June 2020; accepted 23 July 2020

Abstract

The Kuroshio intrusion in a quasi-global eddy-resolving model (LICOMH) and a fully air-sea coupled model (LICOMHC) was evaluated against observations. We found that the Kuroshio intrusion was exaggerated in the former, while biases were significantly attenuated in the latter. Luzon Strait transport (LST) in winter was reduced from -8.8×10^6 m^3/s in LICOMH to -6.0×10^6 m^3/s in LICOMHC. Further analysis showed that different LST values could be explained by different large-scale and local surface wind stresses and the eddies east to the Luzon Strait as well. The relatively stronger cyclonic eddies in LICOMH northeast of the Luzon Island led to weak Kuroshio transport and strong intrusion through the Luzon Strait. The summed transport of all three factors was approximately 2.0×10^6 m^3/s, which was comparable with the difference in LST between the two experiments. The EKE budget showed that strong EKE transport and the baroclinic transformation term led to strong cyclonic eddies east of the Kuroshio in LICOMH, while surface winds contributed little to the differences in the eddies.

Key words: Kuroshio intrusion, South China Sea, eddy-resolving model, air-sea coupled model

Citation: Yang Qian, Liu Hailong, Lin Pengfei, Li Yiwen. 2020. Kuroshio intrusion in the Luzon Strait in an eddy-resolving ocean model and air-sea coupled model. Acta Oceanologica Sinica, 39(11): 52–68, doi: 10.1007/s13131-020-1670-5

1 Introduction

The Luzon Strait (LS), located between the Luzon Island and the Taiwan Island, is a primary gap of the South China Sea (SCS) that forms a connection with the western North Pacific. The Kuroshio, the northward western boundary current of the subtropical gyre of the North Pacific, commonly intrudes westward into the SCS through the LS via various pathways. Sometimes, the intrusion may induce a loop current in the LS, and Kuroshio water flows out of the SCS through the northern part of the LS. The Kuroshio intrusion not only affects stratification (Metzger and Hurlburt, 1996; Qu et al., 2000; Xu and Su, 2000), circulation (Metzger and Hurlburt, 1996; Qu et al., 2000; Xu and Su, 2000; Tian et al., 2006), and mesoscale eddies (Sun et al., 2016) in the northern SCS but also affects the mass, heat and salt budgets of the whole SCS basin (Metzger and Hurlburt, 1996; Qu et al., 2000; Xu and Su, 2000).

Recently, some major features of the Kuroshio intrusion have been gradually identified due to an increasing number of *in situ* measurements, high resolution satellite data and numerical products, including intrusion types (Hu et al., 2000; Caruso et al., 2006; Nan et al., 2011a; Nan et al., 2015; Huang et al., 2016), water exchange in the LS (Lan et al., 2004; Tian et al., 2006; Shu et al., 2014), and interactions between the Kuroshio and mesoscale processes (Yuan et al., 2006; Sheu et al., 2010; Zhao and Luo, 2010; Nan et al., 2011b; Lu and Liu, 2013; Lien et al., 2014; Chang et al., 2015; Nan et al., 2015; Kuo et al., 2017). The Kuroshio intrusion into the SCS also has multiscale variability, ranging from seasonal (Qu et al., 2000, 2004; Xu and Su, 2000; Lan et al., 2004; Yang et al., 2013; Huang et al., 2017) to interannual (Kim et al., 2004; Qu et al., 2004; Wang et al., 2006a; Wu, 2013) to decadal (Nan et al., 2013) timescales. All relevant works prior to 2014 were well documented in the review paper by Nan et al. (2015).

The Kuroshio intrusion is usually estimated by Luzon Strait transport (LST) in the upper 400 m or 1 000 m (Qu et al., 2004; Nan et al., 2013) water layer from 18.5°N to 22.0°N along 120.75°E due to the relatively large number of observations. However, LST cannot describe which path the Kuroshio intrusion takes in the northern SCS. Hu et al. (2000) and Caruso et al. (2006) concluded that there were four and five types of paths, respectively. Nan et al. (2011a) and Nan et al. (2015) recently proposed an area-average geostrophic vorticity method (based on satellite data in the southwestern region of Taiwan) to classify the Kuroshio intrusion. Three different types were identified: the leaping path, the looping path and the leaking path. Huang et al. (2016, 2017) further refined the method into two subindices, called the double index (DI). These methods have been effective for identifying Kuroshio intrusion paths in both observational and modeling studies (Nan et al., 2013; Huang et al., 2017).

In addition to observational studies, many theoretical and numerical models have also been used to study the Kuroshio in-

Foundation item: The National Key R&D Program for Developing Basic Sciences under contract Nos 2018YFA0605703, 2016YFC1401401 and 2016YFC1401601; the Strategic Priority Research Program of Chinese Academy of Sciences under contract No. XDB42010404; the National Natural Science Foundation of China under contract Nos 41976026, 41776030, 41931183, 41931182 and 41576026.

*Corresponding author, E-mail: lhl@lasg.iap.ac.cn

trusion (Metzger and Hurlburt, 1996, 2001; Sheremet, 2001; Xue et al., 2004; Yuan and Wang, 2011; Wu and Hsin, 2012; Jan et al., 2017; Kuo et al., 2017). However, great diversity exists in these modeling results due to the complexity of the processes involved as well as biases in the physics used in the models and/or in the forcing datasets. The annual mean LST in the models summarized by Nan et al. (2015) ranged from -0.6×10^6 m^3/s (Metzger, 2003) to -10.2×10^6 m^3/s (Song, 2006). Metzger and Hurlbert (2001) and Huang et al. (2017) also pointed out that the modeled LST and intrusion path were very sensitive to the resolved topography in the LS. Finer grids and more resolved islands led to smaller LST in the models and less looping or leaking intrusion paths.

With the tremendous increases in computing resources in recent years, more studies have begun to use global- or basin-scale eddy-resolving models either with (Nan et al., 2011b) or without data assimilations (Huang et al., 2017) instead of regional or coarse resolution models due to the large impacts of mesoscale eddy activities on the Kuroshio intrusion (Yuan et al., 2006; Sheu et al., 2010; Zhao and Luo, 2010; Nan et al., 2011b; Lien et al., 2014; Chang et al., 2015; Nan et al., 2015; Kuo et al., 2017). It is likely that circulation becomes more complicated when the models can resolve mesoscale eddies. Therefore, it is necessary to systematically evaluate the Kuroshio intrusion in eddy-resolving models.

Moreover, eddy-resolving models generally tend to simulate stronger eddy activities globally (Masumoto et al., 2004; Yu et al., 2012) and around the LS (Lin et al., 2015; Sun et al., 2016), which is always attributed to insufficient subgrid scale diffusion. The recent works of Renault et al. (2016), Ma et al. (2016) and Feng et al. (2017) all suggested that eddy kinetic energy is significantly reduced in air-sea coupled models due to current feedback or eddy potential energy (EPE) reduction (or both). However, we note that the processes considered in these studies greatly differ. It is also necessary to investigate the simulation of the Kuroshio intrusion in a coupled model.

In the present study, the Kuroshio intrusion in a quasi-global eddy-resolving model and an air-sea coupled model was systemically compared and evaluated against observations. The LST biases in the coupled model were significantly reduced. Differences in the Kuroshio intrusion between the two models could be explained primarily by differences in large-scale surface winds over the Pacific, local surface wind around the LS, and eddy fields. The rest of the paper is organized as follows. Section 2 introduces the datasets. Section 3 presents the Kuroshio intrusion in the two models. Section 4 and Section 5 focus on possible mechanisms to explain the differences between the two models, including remote and local surface wind stress, the pressure gradient between the Pacific and SCS, and mesoscale eddies. In Section 6, we further investigate the mechanisms leading to different eddy fields in terms of budgets. Finally, the discussion and conclusions are provided in Section 7.

2 The numerical models, experiments and observational datasets

2.1 *Models and experiments*

The eddy-resolving oceanic general circulation model (OGCM) that was used in the present study was the State Key Laboratory of Numerical Modeling for Atmospheric Sciences and Geophysical Fluid Dynamics/Institute of Atmospheric Physics (LASG/IAP) Climate System Ocean Model version 2.0 (LICOM2.0) (Liu et al., 2012). To avoid the singularity of the North Pole in the longitude-latitude grid, the model domain extended from 79°S to 66°N. The horizontal grid spacing was uniformly 0.1° with 55 vertical levels. The upper 300 m consisted of 36 uneven levels that increased with depth.

A 60-year hindcast was conducted after a 12-year spinup using climatological forcing from the Ocean Model Intercomparison Project (OMIP; Röske, 2001). For this 60-year period, the model was forced by using the daily Coordinated Ocean-Ice Reference Experiments (COREs) algorithm and data from 1948 to 2007 (Large and Yeager, 2004). Owing to the lack of a sea ice module in LICOM2.0, the sea ice concentration was derived from the observational dataset from the Hadley Center (HadISST, https://climatedataguide.ucar.edu/climate-data/sea-ice-concentration-data-hadisst).

The air-sea coupled model used here mainly consisted of the abovementioned eddy-resolving version of LICOM2.0 and the atmospheric model CAM4 (Community Atmosphere Model version 4), with a 25 km horizontal resolution and 36 vertical levels. The land and sea ice models used in the coupled model were CLM4 (Community Land Model version 4) and CICE4 (Community Ice Code version 4), respectively. The four components were coupled with NCAR Flux Coupler version 7 (Craig et al., 2012). The coupling frequency between the atmosphere and the ocean was 6 h. Because the ocean model excludes the Arctic Ocean, the salinity and potential temperature at the northern boundary are nudged toward the observation of the World Ocean Atlas 2005 (WOA, https://www.nodc.noaa.gov/). The low resolution of this coupled model was described and evaluated in Lin et al. (2016). Here, we called the ocean-only and coupled experiments LICOMH and LICOMHC, respectively. The fully coupled experiment was conducted for 7 a from a quasi-steady state of LICOMH and a CAM spinup. The results from the last 5 years of both experiments were chosen for our analysis.

2.2 *Observational datasets*

Merged satellite altimeter products from the archiving, validation and interpretation of satellite oceanographic (AVISO, http://www.aviso.oceanobs.com) dataset were used in this study for the period of 2003–2007 to match the period of the ocean model simulation. The spatial resolution of the data was 0.25°× 0.25°. We averaged the AVISO daily product every 5 d to obtain the pentad averaged data. The absolute dynamic topography (ADT) was calculated by adding the sea level anomaly (SLA) to the mean dynamic topography. The surface currents were obtained with the geostrophic relation. Water depths less than 200 m were excluded from the diagnosis due to errors caused by tidal signals (Yuan et al., 2006; Nan et al., 2011a).

3 The simulations of the Kuroshio intrusion in LICOMH and LICOMHC

Figures 1a–c compare the mean SSH field and related surface geostrophic currents near the LS among the AVISO observation, LICOMH and LICOMHC. The red lines in Fig. 1 are the Kuroshio axis, defined as the contours of zero geostrophic vorticity. In the observation, the Kuroshio axis extended westward to approximately 120.5°E. The annual mean Kuroshio intrusion in the LICOMH reached approximately 119°E, approximately 1.5° west of the observation. The westward velocity vectors around the LS in the LICOMH were also overestimated, consistent with the exaggerated intrusion. However, the Kuroshio intrusion was greatly reduced in the coupled experiment, LICOMHC, in which the Kuroshio axis extended only to approximately 120.5°E.

The Kuroshio intrusion has evident seasonal variability,

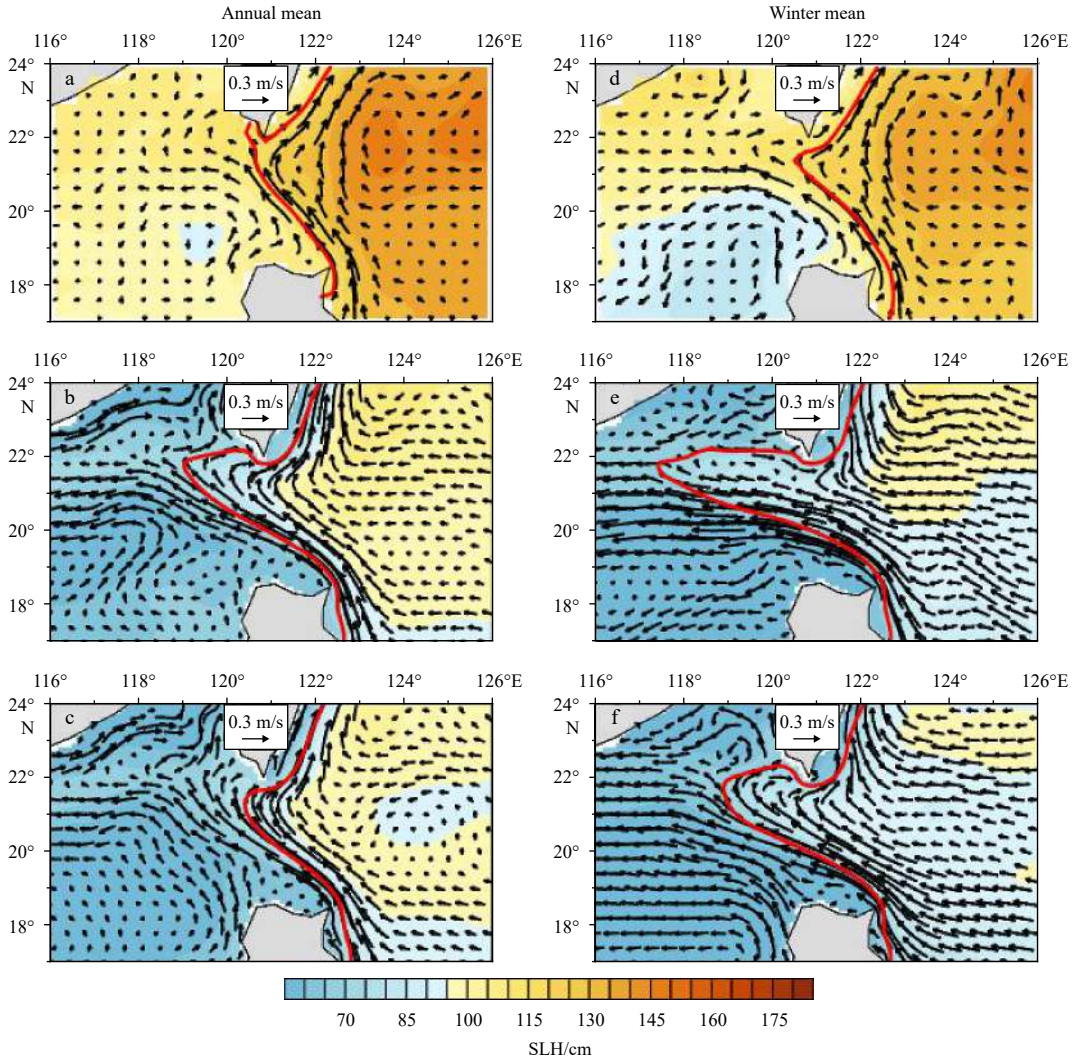

Fig. 1. Annual mean sea level height (shading) and related surface geostrophic currents (vector) near the Luzon Strait for AVISO (a), LICOMH (b) and LICOMHC (c), and the same as a–c but for winter (d–f). The red curve denotes the Kuroshio axis determined by the zero contour of geostrophic vorticity (GV).

being strong in winter and weak in summer (Nan et al., 2015) (Table 1). We further compared the winter intrusion, defined as the average from December to February, in Figs 1d–f. Clearly, the surface current and LST (Table 1) are stronger in winter than the annual mean, while the Kuroshio intrusion was more exaggerated in LICOMH than in LICOMC. The Kuroshio axis in LICOMH extended to approximately 117.5°E, compared to 119°E in LICOMHC. The surface currents were also significantly stronger in the two modeled experiments in winter than the annual mean.

The upper 400 m-integrated currents (both vectors and magnitudes) from these two experiments are also presented (Fig. 2). The annual and winter mean velocity vectors (Figs 2a–b and 2d–e, respectively) resembled the surface geostrophic current shown in Figs 1b–c and 1e–f, confirming the more exaggerated Kuroshio intrusion in LICOMH than in LICOMHC for the upper 400 m. Circulations east of the LS also differed between these two experiments. Generally, the eastward Subtropical Counter Current (STCC) could not be clearly found in LICOMH in the annual

Table 1. The annual and winter mean Luzon Strait transport (LST), defined as the upper 400 m-integrated zonal velocity along 120.75°E from 18.5°N to 22.0°N and the Island rule that was proposed by Godfrey (1989, details in Part 4); and the LST ranges for both the observations and models from Nan et al. (2015)

	LST/10^6 $m^3 \cdot s^{-1}$		LST from Island rule/10^6 $m^3 \cdot s^{-1}$	
	Annual	Winter	Annual	Winter
LICOMH	–5.4	–8.8	–7.1	—
LICOMHC	–4.4	–6.0	–6.0	—
Long-term *in situ* Obs.	–12.4[1)] to –0.5[2)]	–13.7[3)] to –2.75[4)]	–4.0[5)] to –12.4[6)]	—
Numerical models	–10.2[7)] to –0.6[8)]	–12.2[9)] to –3.1[10)]	—	—

Note: [1)] Wang et al. (2006b); [2)] Wyrtki (1961); [3)] Chu and Li (2000); [4)] Wyrtki (1961); [5)] Qu et al. (2004); [6)] Wang et al. (2006b); [7)] Song (2006); [8)] Metzger (2003); [9)] Song (2006); [10)] Rong et al. (2007). — means not available.

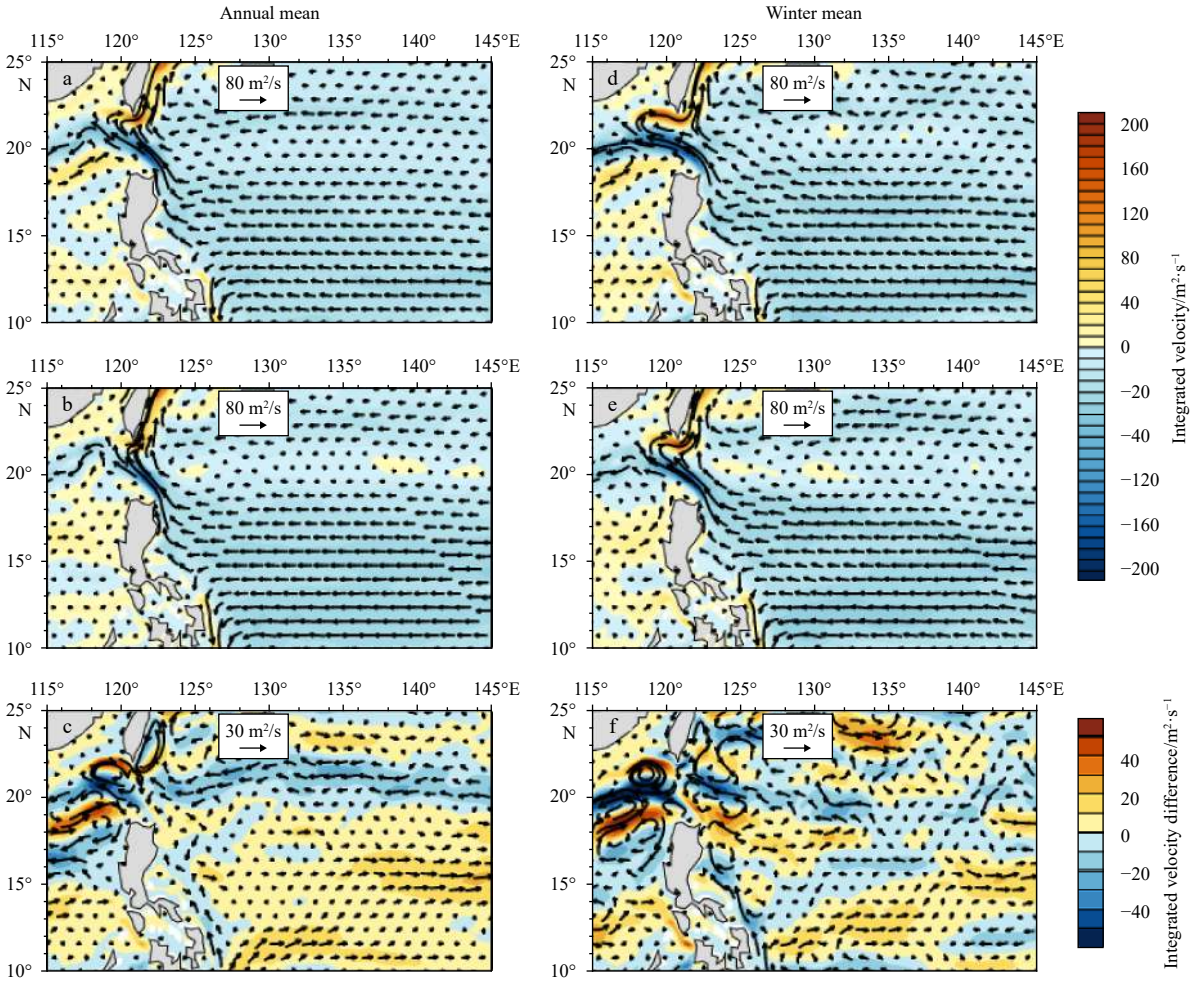

Fig. 2. Annual mean upper 400 m-integrated currents for LICOMH (a) and LICOMHC (b); their differences (LICOMH minus LICOMHC) (c), and the same as a–c but for winter (d–f). The color represents the upper 400 m-integrated zonal velocity.

and winter mean fields (Figs 2a and d), while this current was clearly located at approximately 20.5°N in LICOMHC, which was not the usual location that was noted in the observation. Furthermore, the STCC was only found in LICOMH in the winter mean field east to 130°E, at a location that was approximately 1° north of that in LICOMHC (not shown). The NEC seems to be a bit more northward in LICOMH, so that the Kuroshio intrusion should be weaker in LICOMHC.

The annual and winter circulation differences between LICOMH and LICOMHC (LICOMH minus LICOMHC) are also shown in Figs 2c and f. The annual and winter spatial mean patterns were similar because winter circulation is dominant in this region. The clockwise circulation difference in southwestern Taiwan and weaker upstream Kuroshio both confirmed the stronger intrusion in LICOMH than in LICOMHC. Moreover, the counterclockwise circulation difference at about 18°–21°N east of the LS was related to the missing STCC and weak North Equatorial Current (NEC) at approximately 18°N in LICOMH.

To quantify the intrusion in these two models, we further showed the seasonal cycle of LST in the upper 400 m for these two experiments (Fig. 3). Positive (negative) values represented eastward (westward) transport. The results did not change when the depth was further integrated to the upper 1 000 m (not shown). Table 1 compares the modeled LST with the observed ranges that were tabulated in Nan et al. (2015). The 5-year mean

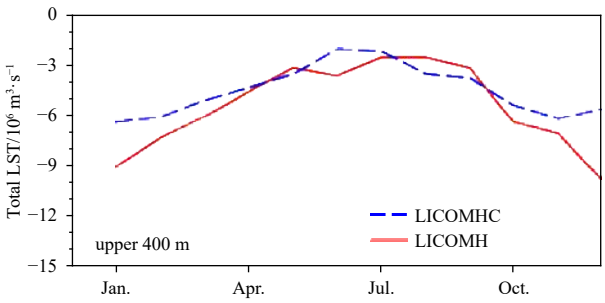

Fig. 3. Seasonal cycle of Luzon Strait transport (LST) for LICOMH (red curve) and LICOMHC (blue curve). Here, LST is defined as the upper 400 m-integrated zonal transport along 120.75°E from 18.5°N to 22.0°N. Positive values represent eastward transport.

modeled LST values were –5.4×10⁶ m³/s and –4.4×10⁶ m³/s in LICOMH and LICOMHC, respectively, both of which were within the observed range, –0.5×10⁶ m³/s to –12.4×10⁶ m³/s (Table 1). The most notable total difference occurred in winter, which was approximately 2.8×10⁶ m³/s. The LST in LICOMHC (–6.0×10⁶ m³/s) was smaller than that in LICOMH (–8.8×10⁶ m³/s) for the upper 400 m (Table 1).

We further investigated the various paths of the Kuroshio intrusion using the DI (the detailed method is presented in Appendix A). The frequencies associated with the three types of Kuroshio paths for LICOMH and LICOMHC and their corresponding LST values are listed in Table 2. We find out that the leaking path dominated in winter. The probability of occurrence of leaking path and looping path in LICOMH is 63.3% and 28.9%, but 54.4% and 33.3% for LICOMHC. This finding indicates that the Kuroshio in winter likely penetrated the SCS (Nan et al., 2015). We further calculated the annual (winter) mean transport when the Kuroshio takes its looping path and leaking path in LICOMH and LICOMHC, respectively. According to Nan et al. (2015), this phenomenon explains why the most notable LST difference between LICOMH and LICOMHC occurs in winter. It is also evident that the looping frequency is increased in LICOMHC, which may be caused by the changes of the local surface wind or circulations within the SCS.

Previous studies have suggested that when the Kuroshio intrusion is relatively weaker, the eddy activity southwest of Taiwan becomes weaker (Nan et al., 2013; Sun et al., 2016) and vice versa. This scenario is also consistent with the weaker intrusion in LICOMHC than in LICOMH, as shown in the surface eddy kinetic energy (EKE) fields (Fig. 4), although both simulations showed much stronger EKE throughout the study region regardless of season compared with the observation (Figs 4a and d). Here, the EKE was calculated as $(u'^2 + v'^2)/2$, where u' and v' are the geo-

Table 2. Occurrence (in front of the slash), which means the total number of occurrence days during the 5 years, and mean LST values (after the slash, 10^6 m/s) for the three types of Kuroshio intrusion paths based on the double index (DI; Huang et al., 2016) method

	Model	Looping frequency/LST	Leaping frequency/LST	Leaking frequency/LST
Annual mean	LICOMH	57(15.6%)/–7.2	48(13.2%)/–4.1	260(71.2%)/–5.3
	LICOMHC	73(20%)/–6.0	51(14.0%)/–4.6	241(66.0%)/–3.9
Winter mean	LICOMH	26(28.9%)/–8.3	7(7.8%)/–7.7	57(63.3%)/–9.1
	LICOMHC	30(33.3%)/–6.3	11(12.2%)/–6.8	49(54.5%)/–5.6

Note: The value in parentheses is the percentage of the frequency for each of the three paths.

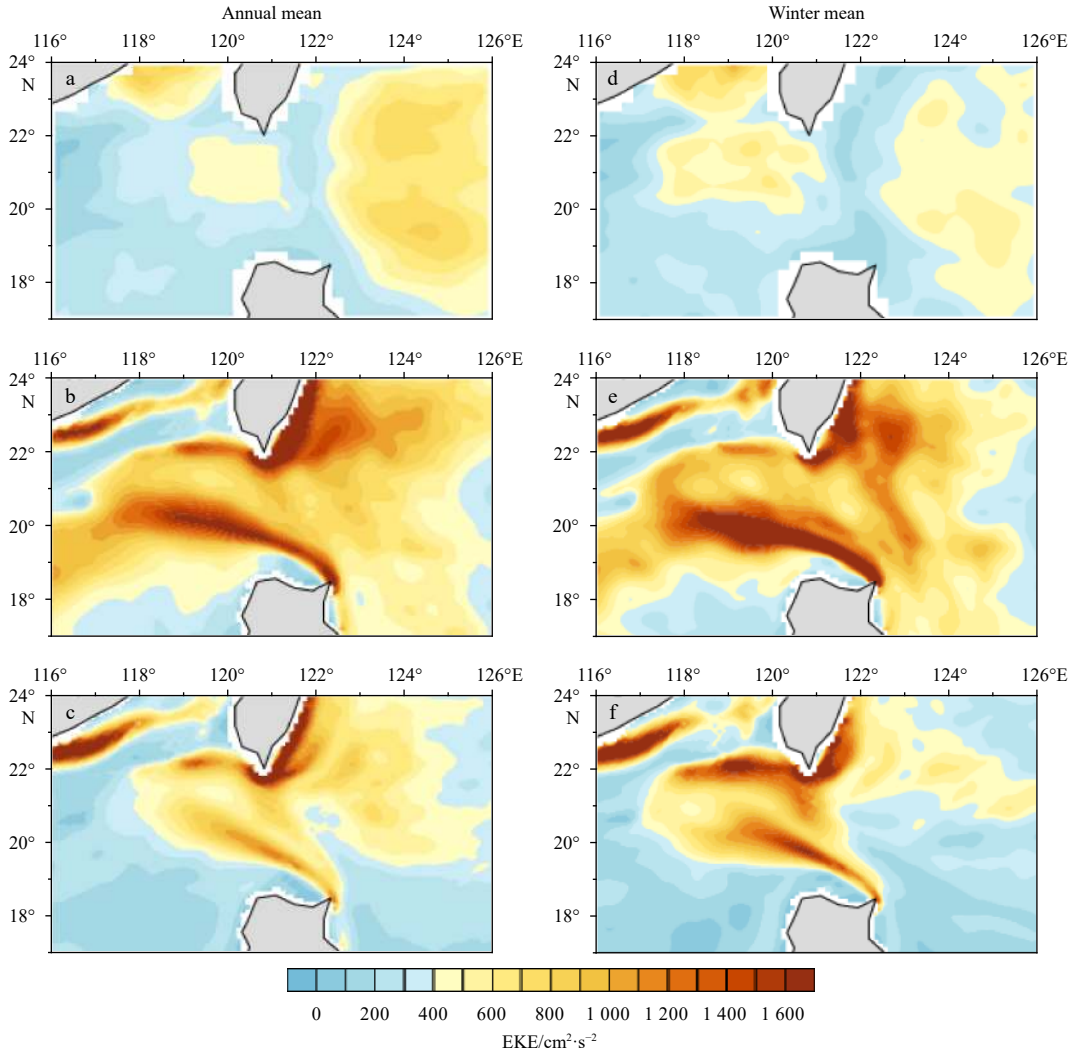

Fig. 4. Annual mean eddy kinetic energy (EKE) for AVISO (a), LICOMH (b), LICOMHC (c), and the same as a–c but for winter (d–f).

strophic velocity anomalies deduced from the SLA.

In summary, we found that the Kuroshio intrusion was exaggerated in the ocean-only model (LICOMH), while the biases were reduced in the fully coupled model (LICOMHC). Since the ocean component in the coupled model was identical to the stand-alone ocean-only model, the changes in the Kuroshio intrusion may have been related to differences in large-scale surface winds (both local and remote) or the pressure gradient between the Pacific Ocean and the SCS between these two experiments. Because the changes of sea surface temperature and currents will affect the atmospheric state in the fully coupled model, including the atmosphere temperature and surface wind. That is, the air-sea interactions tend to dump the large changes of the ocean. In addition, mesoscale eddies in the vicinity of the LS, which are related to intrinsic ocean processes, may also have affected the intrusion, mainly through modifying upstream Kuroshio transport (Lien et al., 2014; Nan et al., 2015). The different EKE fields shown in Fig. 4 suggest the different impacts of mesoscale eddies in the two experiments, especially during winter. We will further investigate these potential contributions next.

4 Impact of large-scale and local winds on the Kuroshio intrusion

According to Qu et al. (2000), the impact of large-scale wind stress on the Kuroshio intrusion can be explained by the "island rule" that was proposed by Godfrey (1989). Thus, LST can be expressed as follows:

$$\mathrm{LST} = \oint_{\mathrm{ABCD}} \tau^{(1)} \mathrm{d}l / \left[\rho_0 (f_\mathrm{D} - f_\mathrm{A})\right], \tag{1}$$

where, $\tau^{(1)}$ is the wind stress along ABCD (Fig. 5a). The Coriolis parameters of A and D are f_A and f_D, respectively, A is located at the southern tip of Mindanao at approximately 4.75°N, and D is located at the northernmost Luzon at approximately 18.75°N. B and C represent two points at the same latitudes as A and D on the American coast; ρ_0 is the reference sea-water density (1 030 kg/m^3).

Figure 5 shows the annual mean surface wind stress (vectors) and wind stress curl (WSC) (shaded) for both LICOMH and LICOMHC. The patterns of wind stress were similar to each other in both experiments but the magnitudes were slightly larger in LICOMH. The averaged LST calculated using Eq. (1) was –7.1×10^6 m^3/s in LICOMH, slightly stronger than –6.0×10^6 m^3/s in LICOMHC (Table 1), and this difference can reasonably explain a large part of the modeled LST difference between these two experiments. Although the island rule cannot be used for studying seasonal changes (Yang et al., 2013), it is also important in explaining the winter differences between the two experiments. Therefore, large-scale wind was used in this study to explain the difference in annual mean LST between LICOMH and LICOMHC.

Furthermore, we calculated the volume transport of the simulated upstream Kuroshio along the western coastat around 19.0°N. Other latitudes have also been tested, and the results are basically the same. We found that the transport for the coupled mode (19.01×10^6 m^3/s at 19.0°N) is larger than that for the ocean model (18.78×10^6 m^3/s at 19.0°N) and this will lead to stronger Kuroshio intrusion in LICOMH. The results are basically similar to Fig. 2. Moreover, the WSC can almost describe the NEC bifurcation latitude, so that is also qualitatively same as the results from the island rule.

Different local winds could also have contributed to the LST difference between LICOMH and LICOMHC (Qu et al., 2000; Nan et al., 2013). Figures 6a and b show the annual mean and winter surface wind stress differences (LICOMH-LICOMHC), respectively. Most of the surface wind differences still existed during winter. Strong southward (or southeastward) differences in the LS may drive westward Ekman transport. Therefore, westward Ekman transport in LICOMH may tend to strengthen the LST. We computed the Ekman transport differences along 120.75°E for these two experiments. The annual mean (winter) transport differences reached 0.2×10^6 m^3/s (0.44×10^6 m^3/s), which accounted for approximately 15%–20% of the total transport difference.

In addition to Ekman transport and the island rule, local WSC can also affect the pressure head between the Pacific Ocean and SCS or change the local gradients of the pressure on both sides of the Kuroshio, which can also affect the intrusion through changing the velocity of the upstream Kuroshio. Figures 6c and d show the annual and winter mean surface WSC difference between these two experiments (LICOMH-LICOMHC), with the hatched area representing values above the 95% significance level. The positive differences throughout the LS suggest that sea surface height anomalies tend to be lower in LICOMH due to Ekman pumping, which compensates for the gradient of sea surface height between the open ocean and the SCS, thus potentially reducing LST. So that, the local wind stress was not responsible for the large intrusion bias in LICOMH.

These results suggest that the excessive intrusion in LICOMH can be largely explained by the remote effect of surface winds through the island rule, with 1.1×10^6 m^3/s for the annual mean. Ekman transport associated with surface winds also contributed approximately 0.2×10^6 m^3/s (or 0.44×10^6 m^3/s during winter) to

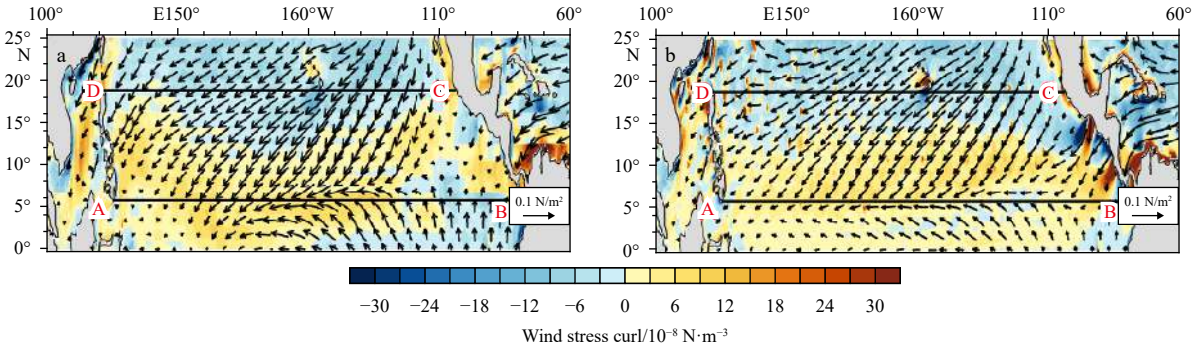

Fig. 5. Annual mean surface wind stress (vector) and wind stress curl (shading) for LICOMH (a) and LICOMHC (b). The ABCD box is the region of integration for the island rule. A is located at the southern tip of Mindanao near 4.75°N, and D is at the northernmost Luzon near 18.75°N; B and C represent two points at the same latitudes as A and D on the American coast.

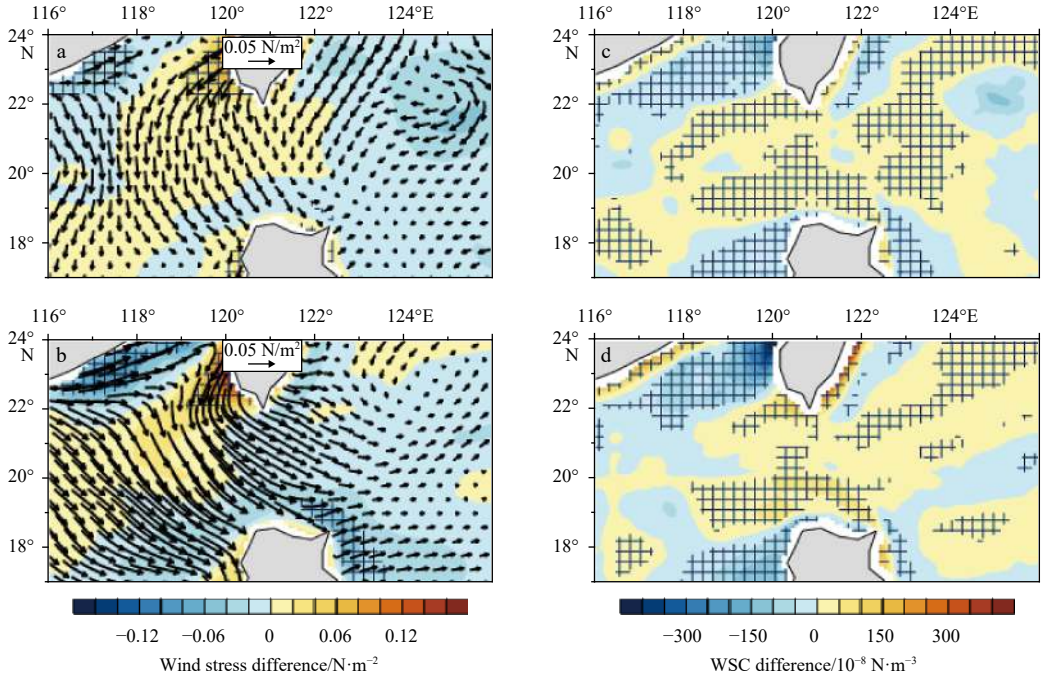

Fig. 6. Differences in surface wind stress (vector) and its magnitude (shading) between LICOMH and LICOMHC (LICOMH minus LICOMHC) for the annual mean (a) and winter mean (b); and the difference in wind stress curl for the annual mean (c) and winter mean (d). The underlined area represents values above the 95% significance level.

the biases, approximately 20% of the LST difference.

5 Effect of eddies on the Kuroshio intrusion

Although the NEC bifurcation is an important candidate affecting the Kuroshio intrusion, the mesoscale eddies can also contribute to part of the changes of KI. Previous studies suggested that cyclonic eddies (CEs) and anticyclonic eddies (AEs) east of Luzon Island may weaken and strengthen the velocity of Kuroshio east of the LS, respectively (Chang et al., 2015). Weaker (stronger) Kuroshio transport will consequently result in a looping (leaping) path (Sheu et al., 2010) and lead to a stronger (weaker) intrusion. Figure 4 shows that the eddy activity east of Luzon was more intense in LICOMH, thus potentially influencing the Kuroshio intrusion.

We use the eddy detection and tracking method of Lin et al. (2007) to categorize eddies in the present study (detailed in Appendix B). Here, we focused on eddies with lifetimes longer than 5 weeks and amplitudes greater than 3 cm. Figure 7 shows the annual and winter mean EKE due to CEs and AEs for LICOMH and LICOMHC in a 1° box. The EKE in the region just west of 121°E and at approximately 124°E was significantly larger in LICOMH than in LICOMHC, particularly during winter. In the upstream region of (18.5°–20.5°N, 123.5°–125.5°E), called northeast of Luzon (NEL), the winter average EKE values due to CEs were 598 cm^2/s^2 and 220 cm^2/s^2 in LICOMH and LICOMHC, respectively (Table 3). Intensive CEs in the NEL region reduced upstream Kuroshio transport and increased the intrusion in LICOMH. However, the EKE due to AEs in the NEL region still differed between these two experiments, but the magnitude was less than that of CEs, especially in winter, as shown in Table 3.

The larger EKE in LICOMH may likely be due to the much stronger intensity and frequency of eddies. Figures 8 and 9 show the annual and winter mean occurrence number and intensity of CEs and AEs for the two experiments. The occurrence number of CEs had some differences in general, and the intensity in LICOMH in the NEL region was much higher than that in LICOMHC. The AE results were also consistent, but the difference was small between the two models. During the 5-year integration, we found 305 (1 210) CEs in the NEL region in LICOMH and 220 (1 430) in LICOMHC in winter (5 a) (Table 3). According to the trajectories of these eddies, most were propagated from the STCC region east of the LS (not shown). The location of the large difference due to CEs was colocated with cyclonic circulation anomalies of the mean flow (Figs 2c and f), indicating the westward propagation of CEs in LICOMH is much stronger.

The difference was much more evident in intensity: approximately 23 cm (23 cm) and 15 cm (19 cm) in the NEL region in winter (composite mean during 5 a) for LICOMH and LICOMHC, respectively (Figs 8c and d, Table 3). Moreover, the 15 cm contours in the NEL region were more westward in LICOMH (approximately 123.5°E for 5 a and 121.5°E in winter) than in LICOMHC (approximately 125°E for 5 a and 123°E in winter) (Figs 8c and d). This result suggests that stronger CEs in LICOMH contributed to the stronger modeled Kuroshio intrusion.

To further analyze the impacts of eddies on the Kuroshio intrusion, we performed a composite SLA and corresponding surface geostrophic current analysis according to the polarity of eddies occurring in the NEL region (Table 3). Figures 10 and 11 show the composite SLA and associated surface geostrophic currents when AEs and CEs occurred in the NEL region, during winter and the 5 years, respectively, and the seasonal circulation was subtracted. We confirmed that eddies affected the Kuroshio intrusion in the models, and the intrusions were significantly stronger when CEs occurred than when AEs occurred, especially in winter. From Fig. 10, the anomaly circulation of Kuroshio was the same as the weak looping path when AEs occurred in the NEL region, while strong transport occurred all the way to the entrance of the SCS (similar to the leaking path) when CEs oc-

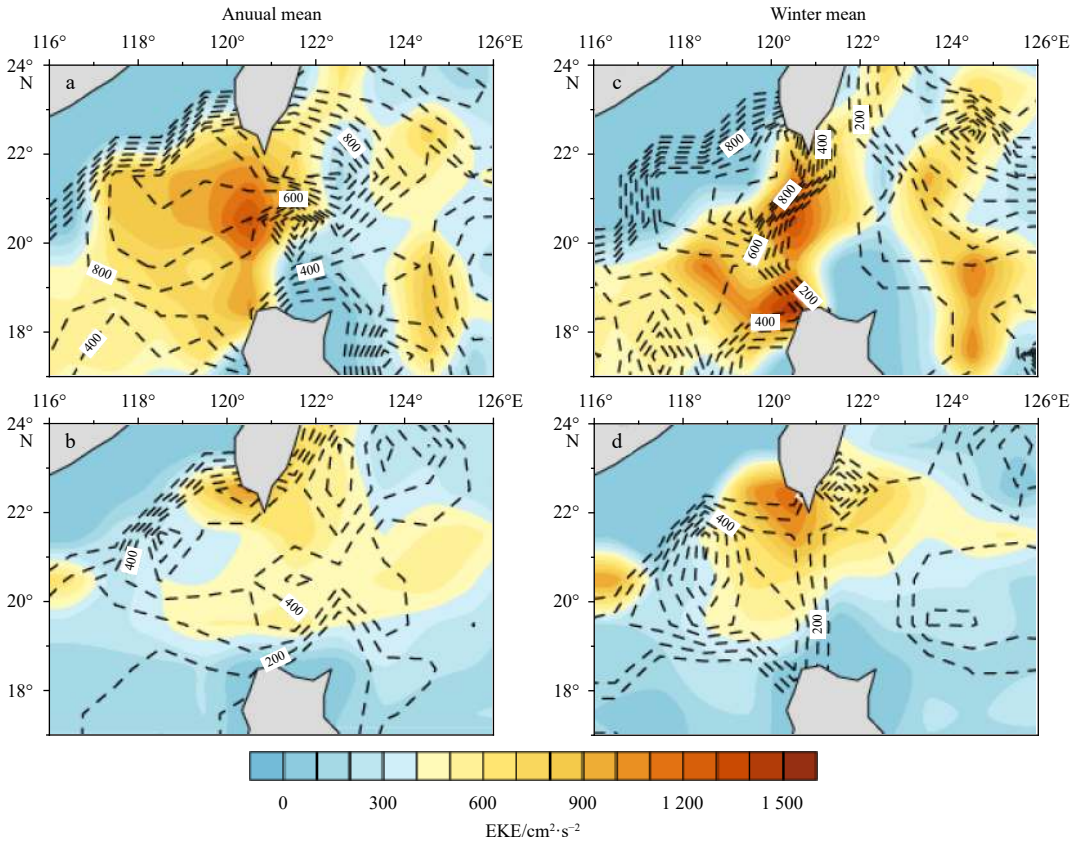

Fig. 7. Composite mean EKE due to cyclonic (shading) and anticyclonic eddies (contours) in LICOMH (a) and LICOMHC (b), and the same as a and b but for winter (c and d).

Table 3. The area-averaged EKE, total occurrence number, mean amplitude and LST change due to both AEs and CEs throughout the key region (18.5°–20.5°N, 123.5°–125.5°E) northeast of the Luzon Strait during the 5 years (in front of the slash) and winters (after the slash) for the two models

		EKE/ $cm^2 \cdot s^{-2}$	Occurrence number	Amplitude/cm	LST change/10^6 $m^3 \cdot s^{-1}$
LICOMH	AE	352/221	1 095/255	18/14	0.2/0.7
	CE	471/598	1 210/305	23/23	–0.1/–1.2
LICOMHC	AE	259/206	1 135/190	17/19	–0.4/0.4
	CE	350/220	1 430/220	19/15	0.7/0.3

curred in LICOMH. However, in LICOMHC, a weak looping pattern was found when CEs occurred, and the intrusion seemed to be weaker than the mean state in Figs 1f and 2f. The pattern looked similar to the leaping path during AE occurrence, and transport anomalies entered the SCS at the northern part of the LS at approximately 22°N. Strong CE circulation in the SCS during AEs occurred in the NEL region in both LICOMH and LICOMHC, hindering the Kuroshio from intruding through the LS. Thus, CEs east of the LS strengthened the Kuroshio intrusion, while AEs weakened it (Zhao and Luo, 2010; Lien et al., 2014; Chang et al., 2015; Nan et al., 2015). The results for the composite mean (Fig. 11) were basically the same, but the enhancement (reduction) of intrusion brought by CEs (AEs) was obviously weaker. It is reasonable to compare the effects related to mesoscale eddies through LST. In this way, we calculated the change in LST when mesoscale eddies occurred in the NEL region (Table 3). The difference in LST caused by eddies in LICOMH was 0.2×10^6 m^3/s stronger than that in LICOMHC in the composite mean state during 5 a, and the difference was 1.2×10^6 m^3/s stronger during winter.

In addition, we investigated the evolution of LST when CEs occurred in the NEL region during winter. The LICOMH and LICOMHC scenarios are shown in Figs 12 and 13, respectively. When comparing with the winter mean state, the spatial scale for the westward transport caused by CEs in LICOMH was apparently stronger than that in LICOMHC. The LST anomalies due to CEs were -1.1×10^6 m^3/s for LICOMH and -0.5×10^6 m^3/s for LICOMHC for the study cases. Thus far, we may certainly conclude that different CEs east of the LS between the two models contributed significantly to the difference in LST between the two models.

The above analysis showed that due to the difference in mesoscale eddies simulated in LICOMH and LICOMHC, the enhancement of the Kuroshio intrusion caused by mesoscale eddies in LICOMH was stronger, which could partly explain the difference in intrusion between the two modes.

6 EKE budget

As mentioned previously, the strengthening effect of CEs on the Kuroshio intrusion was stronger in LICOMH than in LICOM-

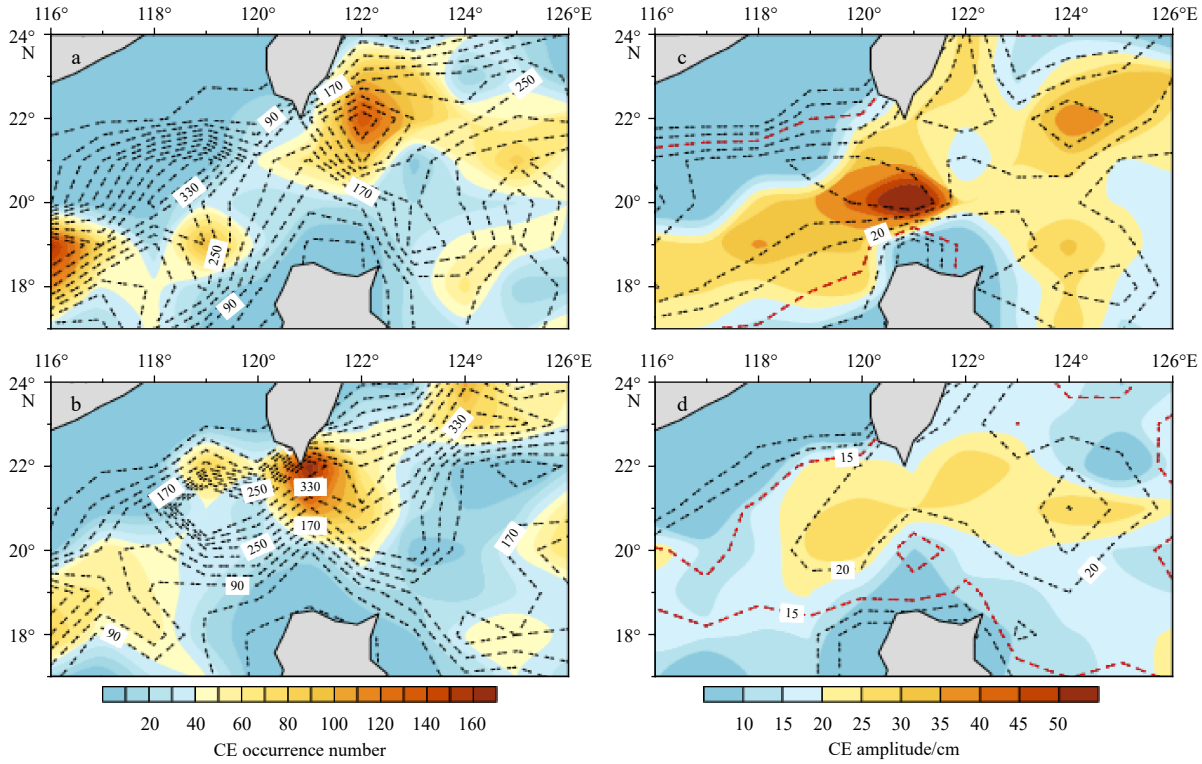

Fig. 8. Occurrence number of cyclonic eddies for LICOMH (a) and LICOMHC (b) during winter (shading) and for the 5 years (contours); and the amplitude of cyclonic eddies (cm) for LICOMH (c) and LICOMHC (d) during winter (shading) and for the 5 years (contours). The interval of the contours in a and b is 40, the interval of the contours is 5 cm, and the 15-cm contours have been highlighted in c and d.

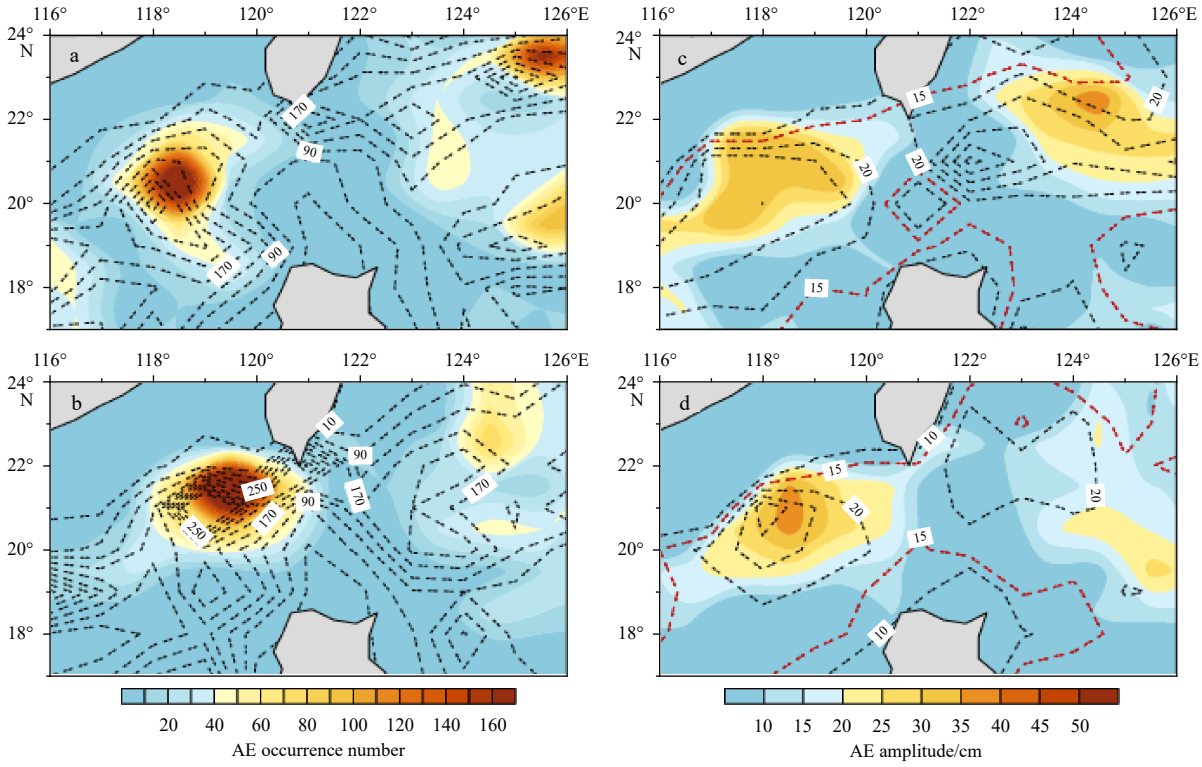

Fig. 9. Occurrence number of anticyclonic eddies for LICOMH (a) and LICOMHC (b) during winter (shading) and for the 5 years (contours); and the amplitude of cyclonic eddies (cm) for LICOMH (c) and LICOMHC (d) during winter (shading) and for the 5 years (contours). The interval of the contours in a and b is 40, the interval of the contours is 5 cm and the 15-cm contours have been highlighted in c and d.

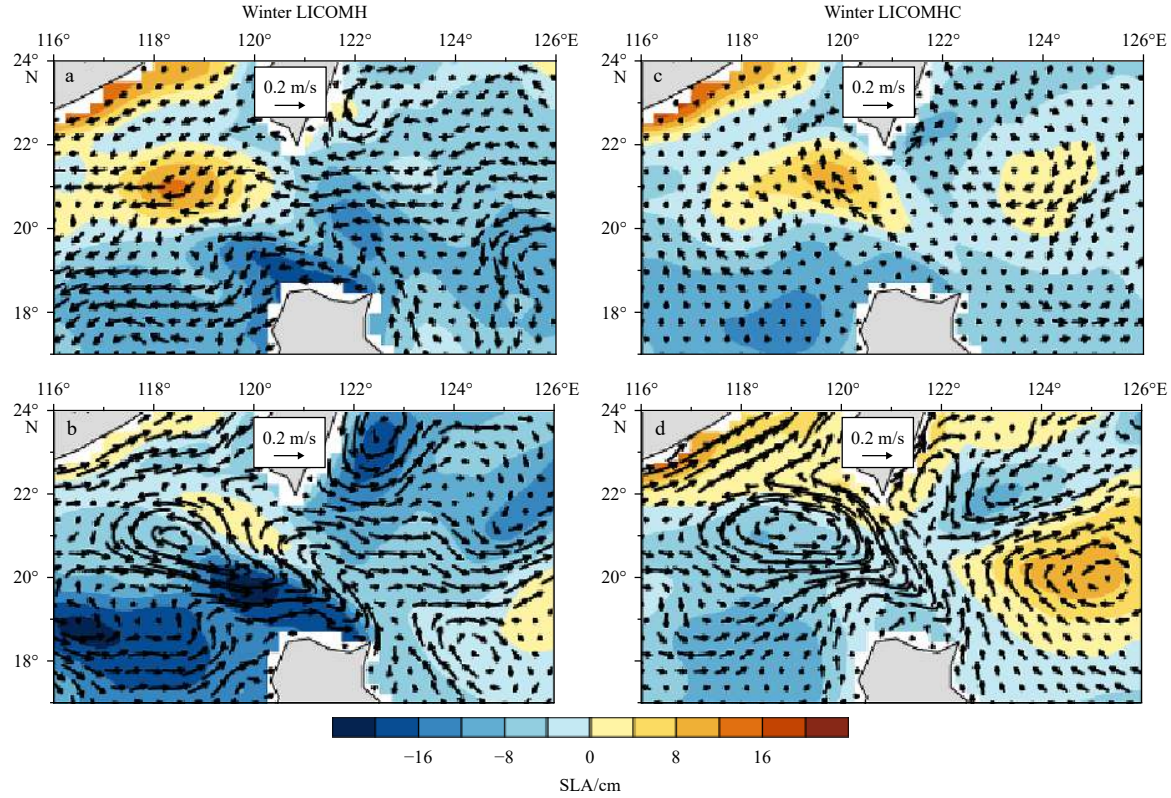

Fig. 10. Composite SLA (shading) and geostrophic current anomalies (vector) (subtracting the climatology) when CEs (a) and AEs (b) occurred in the key region (18.5°–20.5°N, 123.5°–125.5°E) northeast of the Luzon Strait for LICOMH during winter, and the same as a and b but for LICOMHC (c and d).

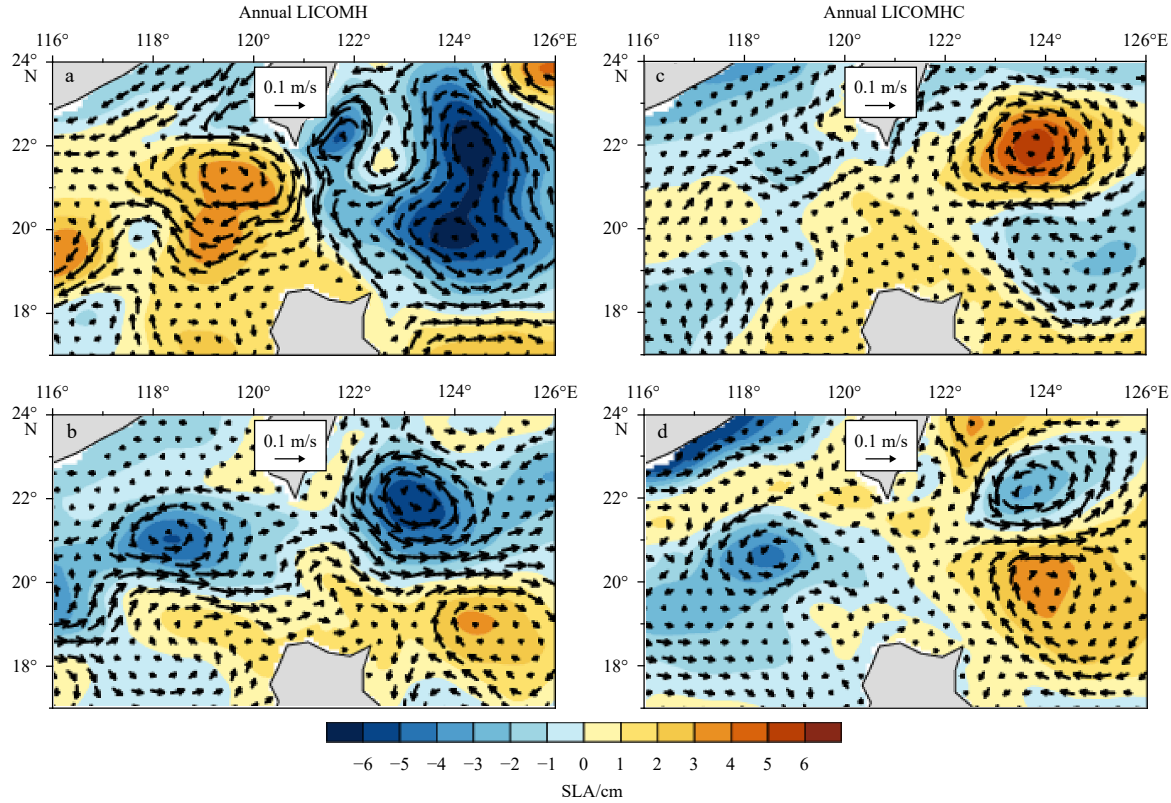

Fig. 11. Composite mean SLA (shading) and geostrophic current anomalies (vector) (subtracting the climatology) when CEs (a) and AEs (b) occurred in the key region (18.5°–20.5°N, 123.5°–125.5°E) northeast of the Luzon Strait throughout the 5-year analysis period for LICOMH; and the same as a and b but for LICOMHC (c and d).

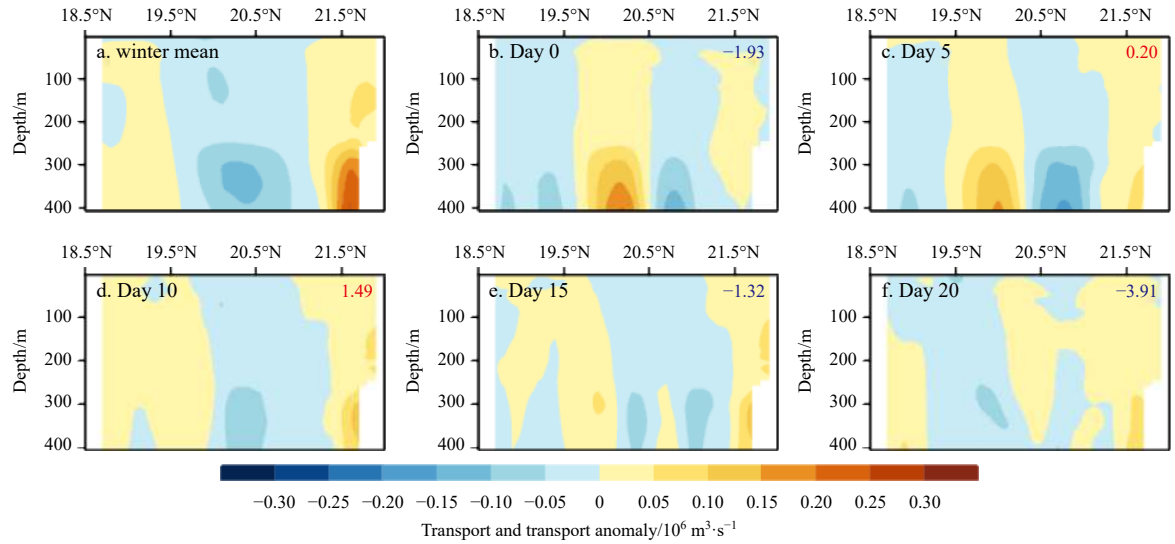

Fig. 12. Winter mean zonal transport along 120.75°E for LICOMH (a); the zonal transport anomalies along 120.75°E when CEs occurred in the key region (18.5°–20.5°N, 123.5°–125.5°E) from January 31 to February 20, 2004 (b–h). The number at the upper right corner of each panel represents an LST anomaly.

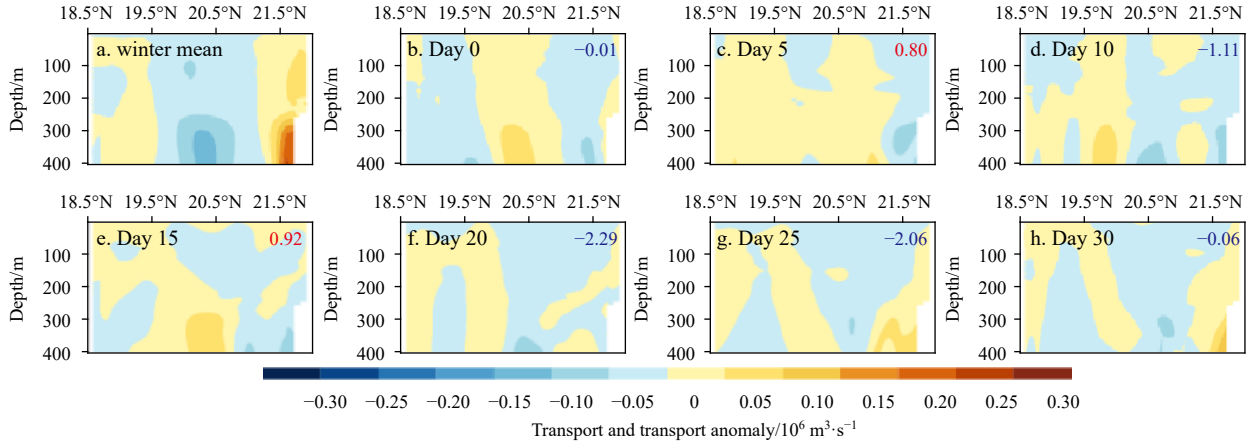

Fig. 13. Winter mean zonal transportalong 120.75°E for LICOMHC (a); the zonal transport anomalies along 120.75°E when CEs occurred in the key region (18.5°–20.5°N, 123.5°–125.5°E) from December 7, 2004 to January 6, 2005. The number at the upper right corner of each panel represents an LST anomaly.

HC. This result implies that less EKE was dissipated, more kinetic energy was transferred from the mean flow or more kinetic energy was transported from other regions. To understand the difference in eddies, the EKE budget for each CE in the NEL region was calculated following Chen et al. (2014), which can be used to explain the transport and transformation of EKE change. The details of the method are shown in Appendix C. Here, we primarily investigated the rate of EKE due to the redistribution caused by horizontal advection (A_{KE}), the energy transformation between eddy potential energy (EAPE) and EKE (D_{KE}), which is also called baroclinic production if the D_{KE} is positive (von Storch et al., 2012), and eddy momentum fluxes (M_{KE}) through barotropic instability.

The annual and winter mean vertically integrated A_{KE}, D_{KE} and M_{KE} in the upper 400 m for LICOMH and LICOMHC are shown in Fig. 14. The area-averaged values of the three terms throughout the NEL region are listed in Table 4.

We found that large values of these terms occurred either along the boundary or along the Kuroshio. In the LS, the balances were between the rate of EKE advection and the transformation of barotropic instability, but the rates of EKE due to baroclinic instability were relatively small (Fig. 14). That is, the EKE generated by horizontal velocity shear was transported by currents outside this region. The comparison between the two models showed that there was more EKE transport outside the LS in LICOMH than in LICOMHC.

However, in the NEL region, which is outside of the western boundary, the patches of negative and positive values were scattered throughout the region. We computed the area averages of the three terms in the NEL region during winter (Table 4). The EKE balances in the two experiments differed. In LICOMH, EKE was mainly transported into the region through advection and was generated through baroclinic instability, while the barotropic term was relatively weak. However, in LICOMHC, EKE was generated through the transformation from EAPE and transported outside and dissipated through barotropic processes. We also

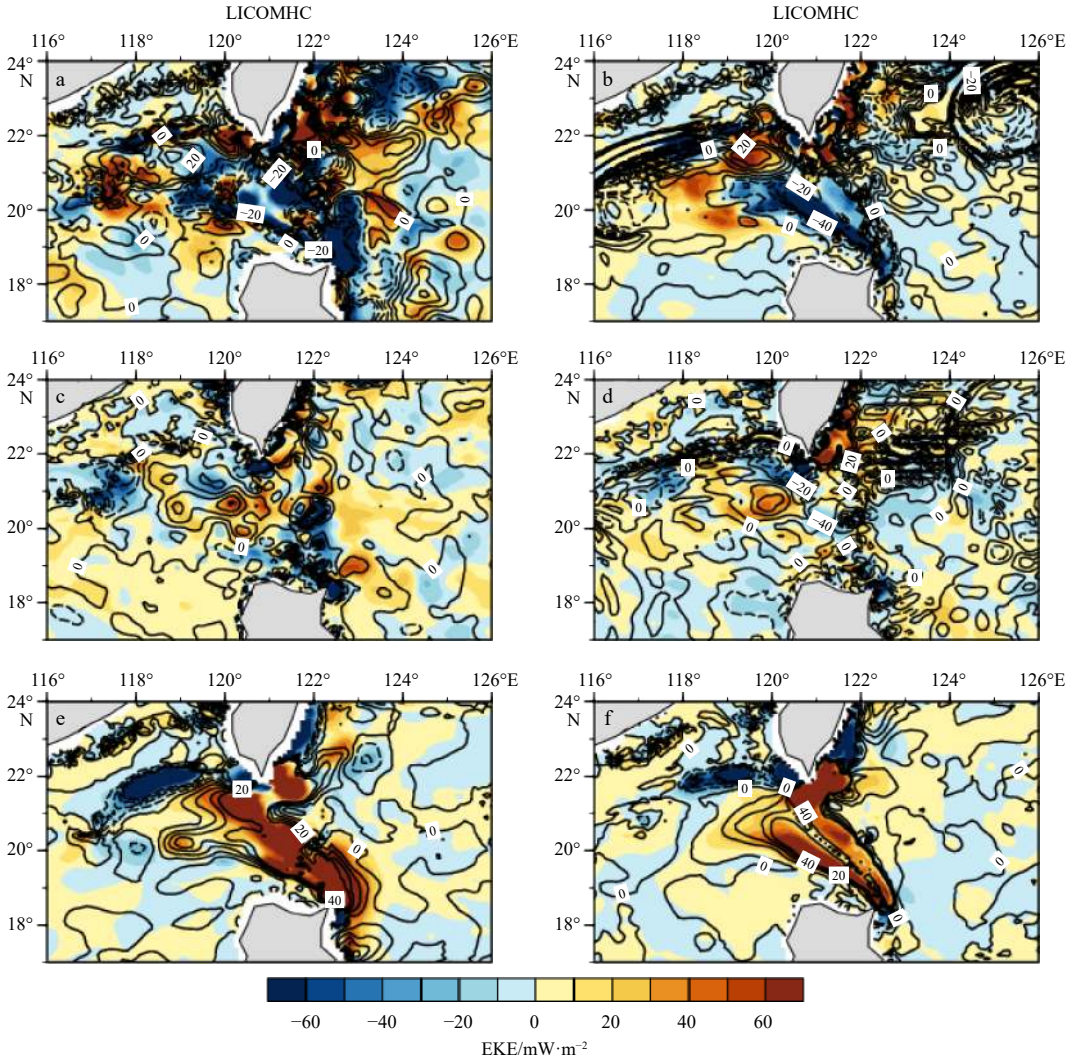

Fig. 14. Upper 400 m-integrated change rate in EKE for each CE in the NEL region due to horizontal advection ($A_{KE,}$ a), baroclinic instability (D_{KE}, c) and eddy momentum flux (M_{KE}, e) for LICOMH during winter (shading), and the contours denote the composite mean values in the 5 years; the same as a, c and e, but for LICOMHC (b, d and f) .

Table 4. The upper 400 m-integrated change rate in EKE due to horizontal advection (A_{KE}), baroclinic instability (D_{KE}) and eddy momentum flux (M_{KE}) for the two models averaged throughout the key region (18.5°–20.5°N, 123.5°–125.5°E) northeast of the Luzon Strait in the composite mean and winter throughout the 5-year analysis period

	A_{KE}/mW·m^{-2}		D_{KE}/mW·m^{-2}		M_{KE}/mW·m^{-2}	
	Annual	Winter	Annual	Winter	Annual	Winter
LICOMH	2.87	4.41	0.30	3.60	–0.53	0.89
LICOMHC	–1.06	–0.44	1.43	0.74	–0.73	–0.55

found that the absolute magnitudes of the main terms, A_{KE} and D_{KE}, were larger in LICOMH than in LICOMHC, indicating strong eddies in LICOMH. The composite mean results in the 5 a were similar, except that EKE dissipation was caused by the barotropic term in LICOMH.

In addition, it has been demonstrated that winds can also dissipate eddy energy (Ferrari and Wunsch, 2009) and can significantly influence mesoscale ocean eddies, especially in energetic western boundary current regions (Xu et al., 2016). Gaube et al. (2015) proposed a formula of the eddy attenuation time scale (T_e):

$$T_e \sim \frac{2\rho_0 D}{3\rho_a C_D U_a} \sim \frac{1}{\sqrt{|\vec{\tau}|}}, \quad (2)$$

where T_e mainly depends on the vertical scale of the mesoscale eddy D, and the wind speed U_a; ρ_0 (1 020 kg/m^3), ρ_a (1.2 kg/m^3), and C_D (1.3×10^{-3}) are surface seawater density, surface air density and the drag coefficient, respectively. Because the differences in D in the two models were very small, we compared the eddy attenuation time scales in LICOMH and LICOMHC by comparing the wind speed. By ignoring the sea surface velocity, T_e is inversely proportional to the reciprocal of the square root of wind stress. That is, the smaller the surface wind stress, the longer the

eddy attenuation time scale and the weaker the dumping effect.

Figure 15 shows the reciprocal of the square root of wind stress for LICOMH and LICOMHC and their differences. The attenuation times for eddies in the annual mean in LICOMH and LICOMHC were approximately the same, but with a relatively large magnitude in LICOMH during winter. We calculated the area average of $1/\sqrt{|\vec{\tau}|}$ differences throughout the NEL region. These differences could be neglected compared with the effects of wind stress in LICOMH and LICOMHC (accounting for approximately 5%). Therefore, local wind was not responsible for the differences in eddies between the two models.

In general, the strong horizontal transport of EKE and strong baroclinic effects in LICOMH led to strong eddies in LICOMH, while surface winds contributed little to the differences in the eddies. The advection term was opposite in the coupled model, and thus, the effect of the air-sea interaction on the EKE balance needs further analysis.

7 Discussion and conclusions

In the present study, the Kuroshio intrusion in a quasi-global eddy-resolving model and an air-sea coupled model was compared and evaluated against observations. The causes of the differences in the Kuroshio intrusion between the two models were explained by differences in large-scale and local surface winds over the tropical Pacific and around the LS, respectively, as well as eddy simulations between the two models. Finally, the balance of EKE was determined to understand differences in the simulated eddies. Interestingly, the Kuroshio intrusion was exaggerated in the ocean-only model, while the biases were significantly attenuated in the fully coupled model. Although the annual mean LST was not significantly reduced in LICOMHC, LST in winter was reduced from –8.8×10^6 m^3/s in LICOMH to –6.0×10^6 m^3/s in LICOMHC, approximately 2.8×10^6 m^3/s less. The transport due to the looping path in LICOMHC was also reduced by approximately 20%, from –8.3×10^6 m^3/s in LICOMH to –6.3×10^6 m^3/s in LICOMHC. The reduction in the Kuroshio intrusion was also demonstrated by other variables, such as the EKE west to the LS.

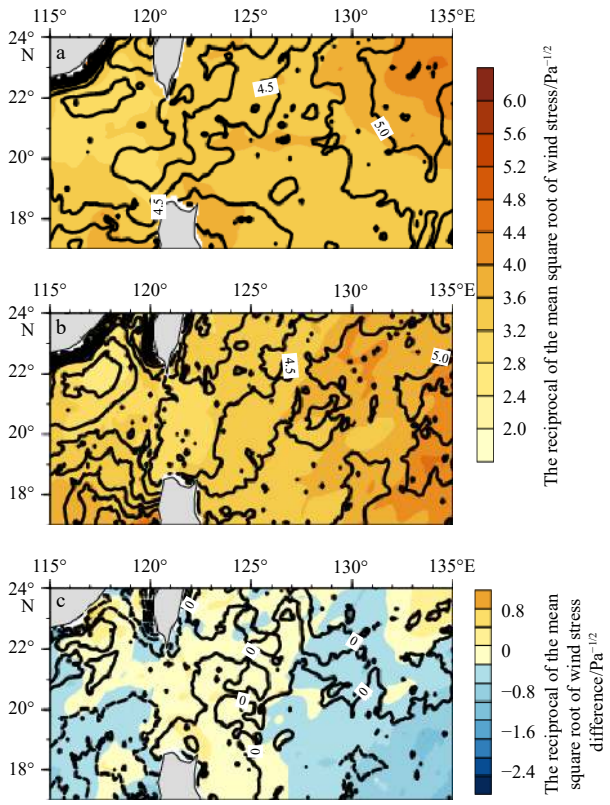

Fig. 15. The reciprocal of the mean square root of wind stress for LICOMH (a) and LICOMHC (b) during winter (shading) and the annual mean (contours), and their difference (LICOMH minus LICOMHC) (c).

The analysis of surface winds showed that the large intrusion could be largely explained by the remote effect of surface winds through the island rule. In addition, local wind stress partially contributed to the difference in LST through Ekman transport and directly changed the upstream speed of the Kuroshio. In addition, weaker CEs in the NEL region in LICOMHC led to a relatively strong Kuroshio and subsequently weakened intrusion, also indicating that a change in the eddy simulation changed the Kuroshio intrusion. Although the remote effect of wind could not be quantified seasonally by using the island rule, the sum of all three factors was approximately 2×10^6 m^3/s, which was comparable with the difference in LST between the two runs in winter.

Further assessment of the EKE budget showed that strong EKE transport, and a strong baroclinic production led to strong CEs in winter east of the Kuroshio in LICOMH. Additionally, the EKE balances east of the Kuroshio were basically different between the two models. The advection and barotropic terms were EKE sinks in the coupled model, while the barotropic effect was slightly weak in LICOMH compared with the other terms. That is, the EKE east of the Kuroshio in LICOMH was transferred from the mean flow and the energy from EAPE. These results were similar to those of Ma et al. (2016), who found that air-sea coupling led to a weak mean flow state via the change in the EKE budget. However, some detailed mechanisms and processes are needed for further investigation.

We also found that there were large differences in the EKE and eddy intensity due to CEs between the two models in the southeastern region of Taiwan (Figs 7 and 8). LST in the presence of CEs east of Taiwan (22.5°–23.5°N, 122.5°–123.5°E) was also computed in the two models (figures not shown). We found that the CEs east of Taiwan in LICOMH led to a more westward intrusion (almost 1°), but LST was slightly weaker than that in LICOMHC. Therefore, the CEs east of Taiwan may have contributed little to part of the Kuroshio intrusion, but these eddies were not a primary factor. This result was different from the study of Chang et al. (2015), who demonstrated that larger numbers of CEs east of Taiwan strengthened the Kuroshio in the LS because of upstream convergence and downstream divergence. However, this finding is also worth further investigation using observational data.

The results also indicate there are biases in the surface wind of CORE dataset in the tropic Pacific Ocean. Recently, Sun et al. (2019) has pointed out that the corrections of surface wind made by CORE lead to a weak NECC in almost all the CORE experiments. The biases in surface wind would result in biases in the volume transports in the tropic Pacific region, and then might affect the transport of Kuroshio and the Kuroshio intrusion in the Luzon Strait. The processes related with the surface wind biases and the exaggerate Kuroshio intrusion need further investigating.

Acknowledgement

We appreciate the constructive comments of Yu-heng Tseng, and acknowledge the technical support from the National Key

Scientific and Technological Infrastructure Project "Earth System Science Numerical Simulator Facility" (EarthLab).

References

Caruso M J, Gawarkiewicz G G, Beardsley R C. 2006. Interannual variability of the Kuroshio intrusion in the South China Sea. Journal of Oceanography, 62(4): 559–575, doi: 10.1007/s10872-006-0076-0

Chaigneau A, Eldin G, Dewitte B. 2009. Eddy activity in the four major upwelling systems from satellite altimetry (1992–2007). Progress in Oceanography, 83(1–4): 117–123

Chang Yulin, Miyazawa Y, Guo Xinyu. 2015. Effects of the STCC eddies on the Kuroshio based on the 20-year JCOPE2 reanalysis results. Progress in Oceanography, 135: 64–76, doi: 10.1016/j.pocean.2015.04.006

Chelton D B, Schlax M G, Samelson R M. 2011. Global observations of nonlinear mesoscale eddies. Progress in Oceanography, 91(2): 167–216

Chen Ru, Flierl G R, Wunsch C. 2014. A description of local and nonlocal eddy–mean flow interaction in a global eddy-permitting state estimate. Journal of Physical Oceanography, 44(9): 2336–2352, doi: 10.1175/JPO-D-14-0009.1

Chen Gengxin, Hou Yijun, Chu Xiaoqing. 2011. Mesoscale eddies in the South China Sea: Mean properties, spatiotemporal variability, and impact on thermohaline structure. Journal of Geophysical Research: Oceans, 116(C6): C06018, doi: 10.1029/2010JC006716

Chu P C, Li Rongfeng. 2000. South China Sea isopycnal-surface circulation. Journal of Physical Oceanography, 30(9): 2419–2438, doi: 10.1175/1520-0485(2000)030<2419:SCSISC>2.0.CO;2

Craig A P, Vertenstein M, Jacob R. 2012. A new flexible coupler for earth system modeling developed for CCSM4 and CESM1. The International Journal of High Performance Computing Applications, 26(1): 31–42, doi: 10.1177/1094342011428141

Feng Baoxin, Liu Hailong, Lin Pengfei, et al. 2017. Meso-scale eddy in the South China Sea simulated by an eddy-resolving ocean model. Acta Oceanologica Sinica, 36(5): 9–25, doi: 10.1007/s13131-017-1058-3

Ferrari R, Wunsch C. 2009. Ocean circulation kinetic energy: Reservoirs, sources, and sinks. Annual Review of Fluid Mechanics, 41: 253–282, doi: 10.1146/annurev.fluid.40.111406.102139

Gaube P, Chelton D B, Samelson R M, et al. 2015. Satellite observations of mesoscale eddy-induced Ekman pumping. Journal of Physical Oceanography, 45(1): 104–132, doi: 10.1175/JPO-D-14-0032.1

Godfrey J S. 1989. A Sverdrup model of the depth-integrated flow for the world ocean allowing for island circulations. Geophysical & Astrophysical Fluid Dynamics, 45(1–2): 89–112

Hu Jianyu, Kawamura H, Hong Huasheng, et al. 2000. A review on the currents in the South China Sea: Seasonal circulation, South China Sea warm current and kuroshio intrusion. Journal of Oceanography, 56(6): 607–624, doi: 10.1023/A:1011117531252

Huang Zhida, Liu Hailong, Hu Jianyu, et al. 2016. A double-index method to classify Kuroshio intrusion paths in the Luzon Strait. Advances in Atmospheric Sciences, 33(6): 715–729, doi: 10.1007/s00376-015-5171-y

Huang Zhida, Liu Hailong, Lin Pengfei, et al. 2017. Influence of island chains on the Kuroshio intrusion in the Luzon Strait. Advances in Atmospheric Sciences, 34(3): 397–410, doi: 10.1007/s00376-016-6159-y

Isern-Fontanet J, García-Ladona E, Font J. 2003. Identification of marine eddies from altimetric maps. Journal of Atmospheric and Oceanic Technology, 20(5): 772–778

Isern-Fontanet J, García-Ladona E, Font J. 2006. Vortices of the mediterranean sea: An altimetric perspective. Journal of Physical Oceanography, 36(1): 87–103

Jan S, Mensah V, Andres M, et al. 2017. Eddy-kuroshio interactions: local and remote effects. Journal of Geophysical Research: Oceans, 122(12): 9744–9764, doi: 10.1002/2017JC013476

Kim Y Y, Qu Tangdong, Jensen T, et al. 2004. Seasonal and interannual variations of the north equatorial current bifurcation in a high-resolution OGCM. Journal of Geophysical Research: Oceans, 109(C3): C03040, doi: 10.1029/2003JC002013

Kuo Yichun, Chern C S, Zheng Zhewen. 2017. Numerical study on the interactions between the Kuroshio current in the Luzon Strait and a mesoscale eddy. Ocean Dynamics, 67(3–4): 369–381, doi: 10.1007/s10236-017-1038-3

Lan Jian, Bao Xianwen, Gao Guoping. 2004. Optimal estimation of zonal velocity and transport through Luzon Strait using variational data assimilation technique. Chinese Journal of Oceanology and Limnology, 22(4): 335–339, doi: 10.1007/BF02843626

Large W G, Yeager S G. 2004. Diurnal to decadal global forcing for ocean and sea-ice models: The data sets and flux climatologies. Boulder: National Center for Atmospheric Research

Lien R C, Ma B, Cheng Y H, et al. 2014. Modulation of Kuroshio transport by mesoscale eddies at the Luzon Strait entrance. Journal of Geophysical Research: Oceans, 119(4): 2129–2142, doi: 10.1002/2013JC009548

Lin Xiayan, Dong Changming, Chen Dake, et al. 2015. Three-dimensional properties of mesoscale eddies in the South China Sea based on eddy-resolving model output. Deep Sea Research Part I: Oceanographic Research Papers, 99: 46–64, doi: 10.1016/j.dsr.2015.01.007

Lin Pengfei, Wang Fang, Chen Yongli, et al. 2007. Temporal and spatial variation characteristics on eddies in the South China Sea: I. Statistical analyses. Haiyang Xuebao, 29(3): 14–22

Lin Pengfei, Liu Hailong, Xue Wei, et al. 2016. A coupled experiment with LICOM2 as the ocean component of CESM1. Journal of Meteorological Research, 30(1): 76–92, doi: 10.1007/s13351-015-5045-3

Liu Hailong, Lin Pengfei, Yu Yongqiang, et al. 2012. The baseline evaluation of LASG/IAP climate system ocean model (LICOM) version 2. Acta Meteorologica Sinica, 26(3): 318–329, doi: 10.1007/s13351-012-0305-y

Lu Jiuyou, Liu Qinyu. 2013. Gap-leaping Kuroshio and blocking westward propagating Rossby wave and eddy in the Luzon Strait. Journal of Geophysical Research Oceans, 118(3): 1170–1181, doi: 10.1002/jgrc.20116

Ma Xiaohui, Jing Zhao, Chang Ping, et al. 2016. Western boundary currents regulated by interaction between ocean eddies and the atmosphere. Nature, 535(7613): 533–537, doi: 10.1038/nature18640

Masumoto Y, Sasaki H, Kagimoto T, et al. 2004. A fifty-year eddy-resolving simulation of the world ocean–preliminary outcomes of OFES (OGCM for the earth simulator). Journal of the earth simulator, 1: 35–56

Metzger E J. 2003. Upper ocean sensitivity to wind forcing in the South China Sea. Journal of Oceanography, 59(6): 783–798, doi: 10.1023/B:JOCE.0000009570.41358.c5

Metzger E J, Hurlburt H E. 1996. Coupled dynamics of the South China Sea, the Sulu Sea, and the Pacific Ocean. Journal of Geophysical Research: Oceans, 101(C5): 12331–12352, doi: 10.1029/95JC03861

Metzger E J, Hurlburt H E. 2001. The importance of high horizontal resolution and accurate coastline geometry in modeling South China Sea Inflow. Geophysical Research Letters, 28(6): 1059–1062, doi: 10.1029/2000GL012396

Nan Feng, Xue Huijie, Chai Fei, et al. 2011a. Identification of different types of Kuroshio intrusion into the South China Sea. Ocean Dynamics, 61(9): 1291–1304, doi: 10.1007/s10236-011-0426-3

Nan Feng, Xue Huijie, Chai Fei, et al. 2013. Weakening of the Kuroshio intrusion into the South China Sea over the past two decades. Journal of Climate, 26(20): 8097–8110, doi: 10.1175/JCLI-D-12-00315.1

Nan Feng, Xue Huijie, Xiu Peng, et al. 2011b. Oceanic eddy formation and propagation southwest of Taiwan. Journal of Geophysical Research: Oceans, 116(C12): C12045, doi: 10.1029/2011JC007386

Nan Feng, Xue Huijie, Yu Fei. 2015. Kuroshio intrusion into the South China Sea: A review. Progress in Oceanography, 137: 314–333,

doi: 10.1016/j.pocean.2014.05.012
Qu Tangdong, Kim Y Y, Yaremchuk M, et al. 2004. Can Luzon Strait transport play a role in conveying the impact of ENSO to the South China Sea. Journal of Climate, 17(18): 3644–3657, doi: 10.1175/1520-0442(2004)017<3644:CLSTPA>2.0.CO;2
Qu Tangdong, Mitsudera H, Yamagata T. 2000. Intrusion of the North Pacific waters into the South China Sea. Journal of Geophysical Research: Oceans, 105(C3): 6415–6424, doi: 10.1029/1999JC900323
Renault L, Molemaker M J, McWilliams J C, et al. 2016. Modulation of wind work by oceanic current interaction with the atmosphere. Journal of Physical Oceanography, 46(6): 1685–1704, doi: 10.1175/JPO-D-15-0232.1
Rong Zengrui, Liu Yuguang, Zong Haibo, et al. 2007. Interannual sea level variability in the South China Sea and its response to ENSO. Global and Planetary Change, 55(4): 257–272, doi: 10.1016/j.gloplacha.2006.08.001
Röske F. 2001. An atlas of surface fluxes based on the ECMWF re-analysis—A climatological dataset to force global ocean general circulation models. Report/Max-Planck-Institut für Meteorologie, 323: doi: 10.17617/2.1560217
Sheremet V A. 2001. Hysteresis of a western boundary current leaping across a gap. Journal of Physical Oceanography, 31(5): 1247–1259, doi: 10.1175/1520-0485(2001)031<1247:HOAWBC>2.0.CO;2
Sheu W J, Wu C R, Oey L Y. 2010. Blocking and westward passage of eddies in the Luzon Strait. Deep Sea Research Part II: Topical Studies in Oceanography, 57(19–20): 1783–1791, doi: 10.1016/j.dsr2.2010.04.004
Shu Yeqiang, Xue Huijie, Wang Dongxiao, et al. 2014. Meridional overturning circulation in the South China Sea envisioned from the high-resolution global reanalysis data GLBa0.08. Journal of Geophysical Research: Oceans, 119(5): 3012–3028, doi: 10.1002/2013JC009583
Song Y T. 2006. Estimation of interbasin transport using ocean bottom pressure: Theory and model for Asian marginal seas. Journal of Geophysical Research: Oceans, 111(C11): C11S19, doi: 10.1029/2005JC003189
Sun Zhikuo, Liu Hailong, Lin Pengfei, et al. 2019. The modeling of the north equatorial countercurrent in the community earth system model and its oceanic component. Journal of Advances in Modeling Earth Systems, 11(2): 531–544, doi: 10.1029/2018MS001521
Sun Zhongbin, Zhang Zhiwei, Zhao Wei, et al. 2016. Interannual modulation of eddy kinetic energy in the northeastern South China Sea as revealed by an eddy resolving OGCM. Journal of Geophysical Research: Oceans, 121(5): 3190–3201, doi: 10.1002/2015JC011497
Tian Jiwei, Yang Qingxuan, Liang Xinfeng, et al. 2006. Observation of Luzon Strait transport. Geophysical Research Letters, 33(19): L19607, doi: 10.1029/2006GL026272
von Storch J S, Eden C, Fast I, et al. 2012. An estimate of the lorenz energy cycle for the world ocean based on the 1/10° STORM/NCEP Simulation. Journal of Physical Oceanography, 42(12): 2185–2205, doi: 10.1175/JPO-D-12-079.1
Wang Dongxiao, Liu Qinyan, Huang Ruixin, et al. 2006a. Interannual variability of the South China Sea throughflow inferred from wind data and an ocean data assimilation product. Geophysical Research Letters, 33(14): L14605, doi: 10.1029/2006GL026316
Wang Yonggang, Fang Guohong, Wei Zexun, et al. 2006b. Interannual variation of the South China Sea circulation and its relation to El Nino, as seen from a variable grid global ocean model. Journal of Geophysical Research: Oceans, 111(C11): C11S14, doi: 10.1029/2005JC003269
Wu C R. 2013. Interannual modulation of the Pacific Decadal Oscillation (PDO) on the low-latitude western North Pacific. Progress in Oceanography, 110: 49–58, doi: 10.1016/j.pocean.2012.12.001
Wu C R, Hsin Y C. 2012. The forcing mechanism leading to the Kuroshio intrusion into the South China Sea. Journal of Geophysical Research: Oceans, 117(C7): C07015, doi: 10.1029/2012JC007968
Wyrtki K. 1961. Physical oceanography of the Southeast Asian waters. Scripps Institution of Oceanography. La Jolla: The University of California, 2: 1–195
Xu Jianping, Su Jilan. 2000. Hydrological analysis of Kuroshio water intrusion into the South China Sea. Acta Oceanologica Sinica, 19(3): 1–21
Xu Chi, Zhai Xiaoming, Shang Xiaodong. 2016. Work done by atmospheric winds on mesoscale ocean eddies. Geophysical Research Letters, 43(23): 12174–112180, doi: 10.1002/2016GL071275
Xue Huijie, Chai Fei, Pettigrew N, et al. 2004. Kuroshio intrusion and the circulation in the South China Sea. Journal of Geophysical Research: Oceans, 109(C2): C02017, doi: 10.1029/2002JC001724
Yang Jiayan, Lin Xiaopei, Wu Dexing. 2013. On the dynamics of the seasonal variation in the South China Sea throughflow transport. Journal of Geophysical Research: Oceans, 118(12): 6854–6866, doi: 10.1002/2013JC009367
Yu Yongqiang, Liu Hailong, Lin Pengfei. 2012. A quasi-global 1/10° eddy-resolving ocean general circulation model and its preliminary results. Chinese Science Bulletin, 57(30): 3908–3916, doi: 10.1007/s11434-012-5234-8
Yuan Dongliang, Han Weiqing, Hu Dunxin. 2006. Surface Kuroshio path in the Luzon Strait area derived from satellite remote sensing data. Journal of Geophysical Research: Oceans, 111(C11): C11007, doi: 10.1029/2005JC003412
Yuan Dongliang, Wang Zheng. 2011. Hysteresis and dynamics of a western boundary current flowing by a gap forced by impingement of mesoscale eddies. Journal of Physical Oceanography, 41(5): 878–888, doi: 10.1175/2010JPO4489.1
Zhao Jie, Luo Dehai. 2010. Response of the kuroshio current to eddies in the luzon strait. Atmospheric and Oceanic Science Letters, 3(3): 160–164, doi: 10.1080/16742834.2010.11446856

Appendix A: The double index method

In this study, the double index (DI) that was defined by Huang et al. (2016) was used to derive the types of Kuroshio intrusion. This index is the areal integral of positive and negative geostrophic vorticity throughout the region (20°–22°N, 119°–121°E) and is named the Kuroshio cold eddy index (KCI) and Kuroshio warm eddy index (KWI). The formulas are as follows:

$$\mathrm{KCI} = \iint \mathrm{sign}\,(\mathrm{GV})\,\mathrm{GV}\mathrm{d}A, \tag{A1}$$

$$\mathrm{KWI} = \iint \mathrm{sign}\,(-\mathrm{GV})\,\mathrm{GV}\mathrm{d}A, \tag{A2}$$

where the sign function and GV are defined as follows:

$$\mathrm{sign}\,(x) = \begin{cases} 1, & x \geqslant 0 \\ 0, & x < 0 \end{cases}, \tag{A3}$$

$$\mathrm{GV} = \frac{\partial v}{\partial x} - \frac{\partial u}{\partial y}. \tag{A4}$$

We used the standard deviations of the two indices as thresholds to obtain the three types of Kuroshio intrusion paths. When the result of the calculation was smaller than the standard deviation of the KWI, the event was defined as a looping path. When the result was greater than the standard deviation of the KCI, the event was defined as a leaping path. The remaining event was a leaking path. In addition, if the looping path and the leaping path both satisfied their criteria, we calculated the normalized result of the two indices. When the absolute value of the normalized KWI (KCI) was large, the event was defined as a looping (leaping) path.

Appendix B: Eddy detection and tracking methods

The eddy detection method that was used in this paper was similar to the WA method (Chaigneau et al., 2009), which has been widely applied in the South China Sea (SCS, Chen et al., 2011; Feng et al., 2017), the Atlantic Ocean (Chaigneau et al., 2009) and broad global oceans (Chelton et al., 2011). First, we identified possible cyclonic eddy (CE) (or anti-cyclonic eddy, AE) centers by searching for local Sea Level Anomaly (SLA) minima (or maxima) in a moving window of 1°×1° grid points. Then, for each possible CE (or AE) center, the algorithm searched for closed contours with an increment (or decrement) of 1 mm. The outermost closed SLA contour that enclosed only the chosen center was considered the eddy edge. According to previous studies (e.g., Chaigneau et al., 2009; Chen et al., 2011), we focused only on eddies with amplitudes greater than 3 cm, lifetimes greater than 5 weeks, and water depths greater than 200 m. The eddy tracking method that was used in this paper was based on the geometrical distance from one eddy center to another (Isern-Fontanet et al., 2003; 2006). The MATLAB code for this method was obtained from Lin et al. (2007) and slightly modified.

When we found eddy centers and edges, some basic eddy properties were estimated, such as amplitude, rotation speed, moving speed and radius. Only the amplitudes were used in the present study, which were defined as the absolute differences in the SLA between the eddy centers and the eddy edges.

Appendix C: Eddy kinetic energy budget

We studied the Eddy Kinetic Energy (EKE) budgets of ocean and coupled model according to Chen et al. (2014).

$$\frac{\partial \mathrm{EKE}}{\partial t} + \nabla \cdot \left(\overline{\vec{u'}\,\overrightarrow{p'}}\right) = A_{\mathrm{K_E}} + D_{\mathrm{K_E}} + M_{\mathrm{K_E}} + \rho_0 \left(\overline{u'D'_u} + \overline{v'D'_v}\right). \tag{A5}$$

The first term on the left-hand side of Eq. (A5) is the temporal change rate of EKE. The second term is the pressure redistribution term. Here, we mainly focused on the first three terms on the right-hand side. The rightmost term represents the change in EKE due to winds, bottom drag and friction. Next, we detailed the physical meaning of these three terms individually.

$$A_{\mathrm{KE}} = -\nabla \cdot \left[\overline{\vec{u}\frac{1}{2}\rho_0\left(u'^2 + v'^2\right)}\right]. \tag{A6}$$

This term represents the EKE redistribution caused by horizontal advection. Note that positive (negative) A_{KE} values indicate means eddy gains (releases) in kinetic energy.

$$D_{\mathrm{KE}} = -g\overline{\rho' w'}. \tag{A7}$$

This term denotes the gain rate of EKE from eddy potential available energy (EAPE) through baroclinic instability. The EAPE is defined as the difference between the potential energy in the instantaneous actual state and that in the time-mean actual state,

EAPE=$-\frac{g}{2n_0}\overline{\rho'(x,y,z,t)^2}$. D_{K_E} will be positive when EAPE is transformed into EKE.

$$M_{K_E} = -\rho_0 \left(\overline{u'\overrightarrow{u'}} \cdot \nabla \bar{u} + \overline{v'\overrightarrow{u'}} \cdot \nabla \bar{v} \right), \tag{A8}$$

where, M_{K_E} indicates the EKE change rate due to eddy momentum fluxes. These changes are caused by barotropic instability, and positive values also indicate eddy gains in EKE.